Antiviral Research 226 (2024) 105897

Contents lists available at ScienceDirect

Antiviral Research

journal homepage: www.elsevier.com/locate/antiviral

Polyoxometalate exerts broad-spectrum activity against human respiratory viruses hampering viral entry

Irene Arduino [a], Rachele Francese [a], Andrea Civra [a], Elisa Feyles [a], Monica Argenziano [b], Marco Volante [c], Roberta Cavalli [b], Ali M. Mougharbel [d], Ulrich Kortz [d], Manuela Donalisio [a,1], David Lembo [a,*,1]

[a] Department of Clinical and Biological Sciences, Laboratory of Molecular Virology and Antiviral Research, University of Turin, Regione Gonzole 10, 10043, Orbassano, Turin, Italy
[b] Department of Drug Science and Technology, University of Turin, Via P. Giuria 9, 10100, Torino, Italy
[c] Department of Oncology, University of Turin, Regione Gonzole 10, 10043, Orbassano, Turin, Italy
[d] School of Science, Constructor University, Campus Ring 1, 28759, Bremen, Germany

ARTICLE INFO

Keywords:
Antiviral agents
Polyoxometalate
Respiratory tract infections
Resistance
Entry inhibitor

ABSTRACT

Human respiratory viruses have an enormous impact on national health systems, societies, and economy due to the rapid airborne transmission and epidemic spread of such pathogens, while effective specific antiviral drugs to counteract infections are still lacking. Here, we identified two Keggin-type polyoxometalates (POMs), $[TiW_{11}CoO_{40}]^{8-}$ ($TiW_{11}Co$) and $[Ti_2PW_{10}O_{40}]^{7-}$ (Ti_2PW_{10}), endowed with broad-spectrum activity against enveloped and non-enveloped human respiratory viruses, i.e., coronavirus (HCoV-OC43), rhinovirus (HRV-A1), respiratory syncytial virus (RSV-A2), and adenovirus (AdV-5). Ti_2PW_{10} showed highly favorable selectivity indexes against all tested viruses (SIs >700), and its antiviral potential was further investigated against human coronaviruses and rhinoviruses. This POM was found to inhibit replication of multiple HCoV and HRV strains, in different cell systems. Ti_2PW_{10} did not affect virus binding or intracellular viral replication, but selectively inhibited the viral entry. Serial passaging of virus in presence of the POM revealed a high barrier to development of Ti_2PW_{10}-resistant variants of HRV-A1 or HCoV-OC43. Moreover, Ti_2PW_{10} was able to inhibit HRV-A1 production in a 3D model of the human nasal epithelium and, importantly, the antiviral treatment did not determine cytotoxicity or tissue damage. A mucoadhesive thermosensitive *in situ* hydrogel formulation for nasal delivery was also developed for Ti_2PW_{10}. Overall, good biocompatibility on cell lines and human nasal epithelia, broad-spectrum activity, and absence of antiviral resistance development reveal the potential of Ti_2PW_{10} as an antiviral candidate for the development of a treatment of acute respiratory viral diseases, warranting further studies to identify the specific target/s of the polyanion and assess its clinical potential.

1. Introduction

Respiratory viruses are the most common cause of infectious diseases and one of the leading causes of morbidity and mortality worldwide, representing a major public health problem and socioeconomical burden (Esneau et al., 2022; Grace et al., 2023; Hadian and Rezayatmand, 2022; Harrington et al., 2021; Ljubin-Sternak et al., 2021). Viral respiratory infections can determine severe complications especially in at-risk populations such as the elderly, infants and immunocompromised subjects, and have been linked to the onset, progression, and exacerbation of asthma and other chronic respiratory diseases in children (Ljubin-Sternak and Meštrović, 2023; Romero-Tapia et al., 2023). Most respiratory viruses still do not have specific antiviral treatments available in clinic settings, and symptoms are usually managed with supportive care. Moreover, an important challenge for antiviral therapy is the emergence of antiviral resistance (Ma et al., 2021; Richman, 2006; Thibaut et al., 2012). Indeed, the high mutation rate and the rapid replication of

* Corresponding author.
E-mail addresses: irene.arduino@unito.it (I. Arduino), rachele.francese@unito.it (R. Francese), andrea.civra@unito.it (A. Civra), elisa.feyles@unito.it (E. Feyles), monica.argenziano@unito.it (M. Argenziano), marco.volante@unito.it (M. Volante), roberta.cavalli@unito.it (R. Cavalli), alismougharbel@gmail.com (A.M. Mougharbel), ukortz@constructor.university (U. Kortz), manuela.donalisio@unito.it (M. Donalisio), david.lembo@unito.it (D. Lembo).
[1] Contributed equally to this work.

https://doi.org/10.1016/j.antiviral.2024.105897
Received 7 February 2024; Received in revised form 22 April 2024; Accepted 25 April 2024
Available online 27 April 2024

Abbreviations

POM polyoxometalate

viruses, coupled with the selective pressure exerted by the antiviral, can lead to the occurrence of mutations in genes encoding for antiviral target sites or antiviral drug activators, that in turn render the antiviral inactive (Feder et al., 2021; Lee and Hurt, 2018).

Polyoxometalates (POMs) are a class of negatively charged inorganic compounds, composed of clusters of oxygen atoms and early transition metal ions in their highest oxidation states, that have recently been investigated in biomedical research as novel therapeutic agents for tumors, bacterial and viral infections, diabetes and Alzheimer's disease (Čolović et al., 2020). The wide spectrum of biological activities of POMs can be ascribed to the structural and compositional variety of these anionic metal-oxo clusters. Indeed, size, structure, shape, redox potential, surface charge distribution, polarity, and acidity of POMs can be easily tuned at the molecular level, consequently affecting their biological activity. In regard to antiviral research, recent studies showed that some POMs are endowed with inhibitory activity against various DNA and RNA viruses, such as human immunodeficiency virus (HIV), herpes simplex viruses (HSV) type 1 and 2, hepatitis viruses type B and C, dengue virus, influenza virus (FluV) A and B and SARS coronavirus (Enderle et al., 2021; Li et al., 2019; Qi et al., 2013, 2020; Wang et al., 2014).

In the present study, we aimed at evaluating the antiviral potential of a selected mini-library of solution-stable POMs, against a panel of human respiratory viruses. In particular, the Anderson-Evans-type POM $[TeW_6O_{24}]^{6-}$ (TeW_6), and the Keggin-type POMs $[TiW_{11}CoC_{40}]^{8-}$ ($TiW_{11}Co$) and $[Ti_2PW_{10}O_{40}]^{7-}$ (Ti_2PW_{10}) were screened for activity against representatives of families of common respiratory viruses, including respiratory syncytial virus (RSV) type A2, human coronavirus (HCoV) type OC43, human rhinovirus (HRV) type A1, and adenovirus (AdV) type 5. This panel included viruses with heterogeneous structural characteristics, such as a naked or enveloped structure, and RNA or DNA genome. Ti_2PW_{10} emerged as the most promising candidate for its broad-spectrum, cell- and strain-independent antiviral activity, and thus was selected for further analyses focused on its antiviral mechanism of action and its tendency to select resistant variants. Furthermore, cytocompatibility and antiviral efficacy of Ti_2PW_{10} were investigated in an in vitro model that closely resembles in vivo conditions, that is, a fully reconstituted 3D model of human nasal epithelium.

2. Materials and methods

2.1. Synthesis of POMs

TeW_6, $TiW_{11}Co$ and Ti_2PW_{10} were prepared following published procedures (Chen, 1997; Domaille and Knoth, 1983; Schmidt et al., 1986). The purity of all POMs was >95%, confirmed by multinuclear NMR spectroscopy (^{31}P and ^{183}W) and infrared spectroscopy.

For biological experiments, POM samples were prepared as suspensions in saline solution (NaCl 0.9% w/v) for the initial biological screening at the starting concentration 930 μM for TeW_6, 617 μM for $TiW_{11}Co$, and 670 μM for Ti_2PW_{10}. Ti_2PW_{10} was prepared at the starting concentration of 5000 μM for later experiments.

2.2. Preparation of rhodamine-labelled Ti_2PW_{10}

Rhodamine-labelled Ti_2PW_{10} was prepared by incubating a rhodamine B aqueous solution with Ti_2PW_{10} under magnetic stirring for 24 h. A dialysis step was carried out (Spectra/Por cellulose membrane, cutoff 1000Da, Spectrum Laboratories, Rancho Dominguez, CA, USA) for 1 h to separate the unbounded rhodamine B. For cell experiments, a colloidal suspension of rhodamine-labelled Ti_2PW_{10} was prepared in saline solution (NaCl 0.9% w/v) at the concentration of 1.34 mM.

2.3. Mucoadhesive thermosensitive in situ hydrogel preparation and characterization

The mucoadhesive thermosensitive *in situ* hydrogel was prepared by a cold method using Pluronic® F127, as thermosensitive polymer, and carboxymethyl cellulose (CMC), as mucoadhesive agent. Pluronic® F127 (20% w/v) was added to ultrapure water under constant gentle stirring and cooled at 4 °C for 24 h to allow the complete dissolution of the polymer. After that, CMC (2% w/v) was added to the solution in an ice bath and the formulation was stored at 4 °C until homogenous solution was obtained. Ti_2PW_{10} was added to Pluronic® F127 solution during the preparation of the *in situ* hydrogel at the concentration of 1.34 mM. The pH of Ti_2PW_{10} formulation was measured at room temperature using a pHmeter Orion model 420A.

Determination of sol to gel transition, rheological analysis, erosion test, and biocompatibility evaluation (hemolysis assay) were performed to characterize the mucoadhesive thermosensitive *in situ* hydrogel formulation, as described in the Supplementary materials.

2.4. Cells and viruses

Human cervix adenocarcinoma epithelial cells (HeLa, ATCC® CCL-2™), human lung fibroblast cells (MRC-5, ATCC® CCL-171™), human epithelial cells (Hep-2, ATCC® CCL-23™), human lung carcinoma epithelial cells (A549, ATCC® CCL-185™), african green monkey fibroblastoid kidney cells (Vero, ATCC® CCL-81™), human hepatocarcinoma cells (Huh7, Cat. N. 01,042,712; European Collection of Authenticated Cell Cultures, ECACC, Public Health England, United Kingdom), human embryonic kidney cells (293T, ATCC® CRL-3216™), and baby hamster kidney cells (BHK21, ATCC® C-13™) were grown in Dulbecco's modified Eagle's medium (DMEM; Sigma-Aldrich) supplemented with 10% (v/v) heat-inactivated fetal bovine serum (FBS; Thermo Fisher Scientific) and with 1% (v/v) antibiotic-antimycotic solution (Sigma-Aldrich), at 37 °C in an atmosphere of 5% CO_2. Fully reconstituted epithelia derived from a mixture of human nasal cells isolated from 14 different donors (MucilAir™-Pool, EP02MP), were purchased from Epithelix Sàrl (Geneva, Switzerland). The tissue inserts were cultured at the air–liquid interface (ALI) with MucilAir™ culture medium (EP05MM), in 24-well plates with 6.5-mm Transwell® inserts (cat #3470, Corning Incorporated, Corning, NY), at 37 °C in an atmosphere of 5% CO_2, according to supplier's instructions.

Human rhinoviruses type A1 (HRV-A1, ATCC® VR-1559) and type B48 (HRV-B48, Cat. N. 0310051v; ECACC), and adenovirus type 5 (AdV-5, ATCC® VR-5™) were propagated on HeLa cells. The laboratory HRV-A1 strains with phenotypic resistance to pleconaril and rupintrivir were previously generated in our laboratory, exhibiting elevated EC_{50}s for pleconaril (>150 μM) and rupintrivir (0.09 μM) (Civra et al., 2022). Human betacoronavirus type OC43 (HCoV-OC43, ATCC® VR-1558™) and alphacoronavirus type 229E (HCoV-229E, 0310051v; ECACC) were cultured on MRC-5 cells. The respiratory syncytial virus A2 strain (RSV-A2, ATCC® VR-1540™) was produced on Hep-2 cells. When cytopathic effect (CPE) developed, cell culture supernatants were clarified, aliquoted, and stored at −70 °C. Viral titers were determined by focus assay (HRV, HCoV) or plaque assay (RSV, AdV) and expressed as focus-/plaque-forming units per mL (FFU/mL and PFU/mL). Virus stock production and all antiviral assays were performed using DMEM supplemented with 2% (v/v) FBS in a humidified 5% CO_2 incubator at 34 °C (HRV, HCoV) or at 37 °C (RSV, AdV), unless stated otherwise. SARS-CoV-2 pseudotyped viruses (SARS-CoV-2 PsV) were produced and titrated with the $TCID_{50}$ (Median Tissue Culture Infectious Dose) method as described in a previous work (Maglione et al., 2023).

2.5. Antiviral assays

The antiviral activity of POMs and POM formulation was assessed via focus (HRV, HCoV) or plaque (RSV, AdV) reduction assays, as previously described (Cagno et al., 2017; Milani et al., 2021). Briefly, confluent cells were added with a fixed viral inoculum (multiplicity of infection, MOI, FFU/cell or PFU/cell: 0.01 for HRV, HCoV, RSV; 0.001 for AdV) and serial dilutions of POM (100–0.12 μM), and then incubated for a variable amount of time depending on the virus. HCoV/HRV-infected plates were incubated for 16h or 24h respectively. Instead, after 2h-incubation of the virus-POM mixture, RSV/AdV-infected plates were overlaid with medium containing 1.2% methylcellulose and serial dilutions of POM for 72h or 120h respectively. After incubation for all described experiments, HRV/HCoV/RSV-infected cells were fixed with cold acetone-methanol (50:50) and subjected to an immunocytochemistry procedure, described in the Supplementary materials. AdV-infected cells were fixed and stained with 0.1% crystal violet in 20% ethanol. The number of infected cells or plaques was microscopically counted and viral infectivity was reported as mean % of untreated control ± standard error of the mean (SEM). For the pre-treatment assays, cells were incubated with serial dilutions of POM for 2h, and then treated as for the focus reduction assay. In the entry assays, after 20-min infection at 4 °C of prechilled cells with a fixed viral inoculum (MOI 0.05) to allow attachment of virus, and three washes with cold medium to remove unbound virus, cells were treated with serial dilutions of Ti_2PW_{10}, and incubated for 1h at 34 °C to allow virus entry. Cells were then subjected to a 30-sec treatment of citrate buffer (pH 3.0) for HCoV-OC43 or 3 washes of PBS++ (PBS with 1 mM $MgCl_2$ and 1 mM $CaCl_2$) for HRV-A1 to inactivate outer virions, washed with warm medium three times, incubated and treated as for the focus reduction assay. In the post-entry assays, cells were infected for 1h (MOI 0.05), incubated with 25 mM of NH_4Cl for 15 min, and treated with serial dilutions of POM in presence of NH_4Cl. The NH_4Cl treatment inhibits endosome acidification and thus blocks viral particles inside the endosome, still allowing the replication of those particles that already escaped from late endosomes (Civra et al., 2018). Cells were then incubated and treated as for the focus reduction assay.

For SARS-CoV-2 PsV assays, Huh7 cells were treated with serial dilutions of POM and after 2h infected with a fixed amount of PsV (8000 $TCID_{50}$/mL) in presence of POM dilutions. Control wells were prepared with only culture medium (CC wells) and infected untreated (VC wells). 20h after infection, the detection was performed with the Britelite plus reporter gene assay system (PerkinElmer, Waltham, MA, USA, cat. no. 6066769) using the Infinite F200 luminescence reader (TECAN, Männedorf, Switzerland). Infectivity (%) was calculated as follows: [(mean RLU of each treated well - mean RLU of CC)/(mean RLU of VC - mean RLU of CC) x 100].

2.6. Cell viability and cytotoxicity assays

Cell viability was measured using the MTS [3-(4,5-dimethylthiazol-2-yl)-5-(3-carboxymethoxyphenyl)-2-(4-sulfophenyl)-2H-tetrazolium] assay, as described elsewhere (Cagno et al., 2015), treating cells with POMs under the same experimental conditions as for the focus reduction assays. Cytotoxicity was assessed via lactate dehydrogenase (LDH) assay, using the CytoTox 96 Non-Radioactive Cytotoxicity Assay kit (Promega, Madison, WI) as previously described (Civra et al., 2022).

2.7. Virus yield reduction assays

Sub-confluent cells were infected (MOI 0.05) in presence of Ti_2PW_{10} or POM formulation (at EC_{99} dose), and incubated until advanced cytopathic effect (CPE) was evident in the control wells. Then, supernatants were harvested and virus titers were determined by focus or plaque assay, as appropriate.

2.8. Binding assays

Cells were infected (MOI 3) with the POM at EC_{90} dose and incubated at 4 °C for 1h, to allow virus binding to the cell surface but preventing the entry. Then, cells were washed twice with cold medium to remove the unbound virus, collected in 200 μL of fresh medium and subjected to three rounds of freeze-thawing to release cell-bound virus. The lysate was clarified and the cell-bound virus titer was determined by focus assay.

2.9. Evaluation of cellular uptake by confocal laser microscopy

Pre-seeded cells on coverslips were treated with rhodamine-labelled Ti_2PW_{10} (at 50 μM) for 5 min, 1 h and 3 h at 34 °C. After incubation, cells were washed with PBS 1X five times and sections of red living cells were taken at the confocal laser microscope (LSM800; Carl Zeiss, Jena, Germany). Images were processed with Zen Software (Carl Zeiss).

2.10. Selection of drug-resistant viruses

The ability of Ti_2PW_{10} to select resistant strains of HRV-A1 or HCoV-OC43 was tested with two different approaches according to published procedures, i.e., serial passages approach (Kaptein et al., 2021) and clonal approach (Lacroix et al., 2015).

For the serial passages approach, 24-well-plate HeLa or MRC-5 cells were inoculated with HRV-A1 or HcoV-OC43 (MOI 0.01), in presence of a 2-fold serial dilution of Ti_2PW_{10}, and incubated at 34 °C. Every day, wells were microscopically monitored for CPE and, when full CPE developed in the control untreated well, the supernatant from treated wells showing 30–70% CPE was collected and pooled. In parallel, untreated HRV-A1 or HcoV-OC43 was passaged using the same procedure, as control. Clarified supernatants were titrated by focus assay and tested for the sensitivity to Ti_2PW_{10} by focus reduction assay. Harvested virus was also used to infect freshly seeded cells, repeating the same procedure for the subsequent passage. The concentrations of compound were gradually increased at each passage. Uninfected treated samples were prepared for each passage, to monitor a possible cytotoxic effect of the treatment.

In the clonal approach, four 96-well plates of HeLa or MRC-5 cells (i.e., 384 wells) were infected with HRV-A1 or HcoV-OC43 (MOI 0.1), and concurrently treated with Ti_2PW_{10} at the EC_{99} dose. Plates were incubated at 34 °C and checked every day until total CPE was observed in the control wells (i.e., 7 days post-infection, d.p.i.). In parallel, uninfected treated controls and infected untreated controls were prepared to exclude any cytotoxic effects due to the treatment and to monitor virus-induced CPE without treatment, respectively. Supernatant of CPE-exhibiting treated wells was harvested; clarified virus was expanded under drug pressure and tested to assess its sensitivity to Ti_2PW_{10} by focus reduction assay.

2.11. Experiments on 3D models of human nasal epithelium

To assess POM antiviral activity, after one wash of the apical side of epithelia with medium, 50,000 FFU of HRV-A1 in a total volume of 100 μL was inoculated apically and incubated for 3h at 34 °C, to allow virus entry. Then, the inoculum was removed by three rapid washing steps, and residual virus was collected in 100 μL of culture medium added to the apical side for 10 min. 20 μL of Ti_2PW_{10} at 50 μM or culture medium as control was added apically to infected epithelia, and incubated at 34 °C for 24h, to allow virus replication. Every 24h, viral progeny was collected apically as above-described, and treatment was repeated. Infectious HRV-A1 titers of daily-harvested virus were determined by focus assay.

Concurrently, toxicity of the antiviral treatment on epithelia was assessed by LDH assay on the basal media of untreated and treated samples collected every 24h after treatment, as outlined above.

Physiological turnover in nasal epithelia was set at a 5% threshold of toxicity (Boda et al., 2018).

At the end of the experiment, epithelia were fixed in buffered formalin and embedded in paraffin. Tissue slices were then haematoxylin/eosin (H&E) stained, to assess tissue morphology after treatment.

2.12. Statistical analyses

Results are reported as mean values of two independent experiments performed in duplicate. Values of EC_{50} (half maximal effective concentration), EC_{90} (90% effective concentration), CC_{50} (half maximal cytotoxic concentration) and respective 95% confidence intervals (CIs) were calculated with GraphPad Prism 9.0 (GraphPad Software, Boston, MA, USA) by regression analysis by fitting a variable slope-sigmoidal dose-response curve. Selectivity indexes (SIs) of POMs were calculated as $SI = CC_{50}/EC_{50}$. Where appropriate, Student's t-test was used to compare virus titers of treated and untreated samples. Significance was reported for p value < 0.05 (*), <0.01 (**) and <0.001 (***).

3. Results

3.1. Solution-stable POMs were synthesized and characterized

The three solution-stable POMs, i.e., the Anderson-Evans type TeW_6, and the Keggin-type $TiW_{11}Co$ and Ti_2PW_{10}, were synthesized following reported procedures. These polyanions were specifically selected due to their known biological activity. In order to confirm their purity, the POM salts were analyzed in the solid state by infrared spectroscopy (IR) and in solution by multinuclear NMR spectroscopy (^{31}P, ^{183}W). The identity of each POM was determined from the fingerprint region of its infrared spectrum (ca 400-1200 cm^{-1}).

3.2. Two polyoxometalates showed broad antiviral activity against a panel of human respiratory viruses in vitro

The antiviral activity of the POMs mini-library was assayed against a selected panel of human respiratory viruses, i.e., HRV-A1, HCoV-OC43, RSV-A2 and AdV-5. As reported in Table 1, the Keggin-type POMs $TiW_{11}Co$ and Ti_2PW_{10} were able to inhibit in a dose-dependent manner all tested viruses, exhibiting EC_{50}s in the low micromolar range (0.65–4.10 μM), whereas the Anderson-type POM TeW_6 was not active against any of the tested viruses. Cell viability assays showed that Ti_2PW_{10} was not toxic at any dose tested on any cell line used (CC_{50}s > 225 μM), while $TiW_{11}Co$ showed cytotoxicity upon long incubation times. Based on this result, we focused subsequent analyses on the POM endowed with the minor cytotoxicity, Ti_2PW_{10}. Of note, the anti-RSV activity of Ti_2PW_{10} observed here was previously investigated by Shigeta et al. (2006), thus excluding RSV-A2 from further studies.

Firstly, we investigated the possible antiproliferative effects of Ti_2PW_{10} via MTT assays, showing CC_{50}s > 2400 μM on different cell lines (HeLa, MRC-5, Huh7, A549, Vero, Hep-2), except for the longest treatment time (120h) on HeLa cells (CC_{50} 613.2 μM) (Fig. S1). In particular, results from the MTT assays reported a >80% cell viability following POM treatment at the highest concentration tested (2400 μM) for HeLa (24h-treatment), MRC-5, A549, and Vero cells, while Huh7, Hep-2, and HeLa (120h-treatment) cells exhibited a >80% viability at 300, 1200, and 150 μM, respectively. Altogether, these data show that does not exert antiproliferative action on cells at antiviral effective doses, with highly favorable SIs. The good cytocompatibility of Ti_2PW_{10} was further confirmed through LDH assays, showing less than 10% cytotoxicity on HeLa and MRC-5 cell lines up to the highest POM concentration tested (2400 μM) (Fig. S2).

The broad-spectrum activity of Ti_2PW_{10} against respiratory viruses was further investigated via virus yield reduction assays. As shown in Fig. 1, both HRV-A1 and HCoV-OC43 infectious progeny production was significantly inhibited by the treatment, with a log titer reduction of 5.5 and 3.4 respectively. Interestingly, Ti_2PW_{10} did not inhibit AdV-5 in this stringent experimental setting, and therefore the adenovirus was not included in subsequent experiments.

Ti_2PW_{10} activity against HRV-A1 and HCoV-OC43 was investigated employing different cell lines (Huh7, A549, Vero), which are known models for in vitro experiments on HRV and HCoV (Fausto et al., 2023; Freymuth et al., 2005; Jin et al., 2023; Jurgeit et al., 2012). As reported in Table 2, the POM was active on all cell lines, indicating that its anti-HRV-A1 and anti-HCoV-OC43 activity was not cell line-dependent. Next, we confirmed Ti_2PW_{10} activity against laboratory strains of HRV-A1 with phenotypical resistance to pleconaril or rupintrivir, previously generated in our laboratory (Civra et al., 2022), and additional strains of HRV and HCoV (HRV-B48, HCoV-229E, SARS-CoV-2) (Table 2). Interestingly, we showed that the closely-related HRV type B48 was less sensitive to Ti_2PW_{10} compared to HRV-A1, with an EC_{50} of 39.5 μM (more than 10-fold higher than that for HRV-A1). Regarding coronaviruses, the alpha-coronavirus HCoV-229E was effectively inhibited by the POM (EC_{50} 0.92 μM). Moreover, we showed that Ti_2PW_{10} inhibited in a dose-dependent manner SARS-CoV-2, using a VSV-based pseudovirion expressing SARS-CoV-2 Spike, with an EC_{50} value of 4.05 μM and a favorable SI (>593). Control experiments were performed with well-known antivirals; in particular, the capsid binder

Table 1
Antiviral activity of POMs against selected respiratory viruses.

Compound	Virus	EC_{50} [a] (μM) (95% CI [b])	EC_{90} [c] (μM) (95% CI)	CC_{50} [d] (μM) (95% CI)	SI [e]
TeW_6	HRV-A1	n.a.	n.a.	n.t.	n.a.
	HCoV-OC43	n.a.	n.a.	n.t.	n.a.
	RSV-A2	n.a.	n.a.	n.t.	n.a.
	AdV-5	n.a.	n.a.	n.t.	n.a.
$TiW_{11}Co$	HRV-A1	2.32 (1.42–3.79)	4.82 (2.73–8.49)	>225	>97.0
	HCoV-OC43	2.30 (1.85–2.83)	13.5 (8.80–21.6)	>225	>97.8
	RSV-A2	4.10 (2.96–5.69)	10.1 (5.08–20.0)	121.8 (96.9–153.3)	29.7
	AdV-5	1.14 (0.92–1.41)	3.78 (1.99–7.15)	118.9 (110.7–127.7)	104.3
Ti_2PW_{10}	HRV-A1	3.21 (2.71–3.81)	5.53 (4.57–7.56)	>225	>70.1
	HCoV-OC43	3.30 (3.12–3.50)	12.7 (11.1–14.4)	>225	>68.2
	RSV-A2	2.88 (2.23–3.72)	8.16 (4.30–15.5)	>225	>78.1
	AdV-5	0.65 (0.47–0.90)	4.37 (2.21–9.70)	>225	>346.2

n.a.: not assessable.
n.t.: not tested.
[a] EC_{50}: half maximal effective concentration.
[b] CI: 95% confidence interval.
[c] EC_{90}: 90% effective concentration.
[d] CC_{50}: half maximal cytotoxic concentration.
[e] SI: selectivity index.

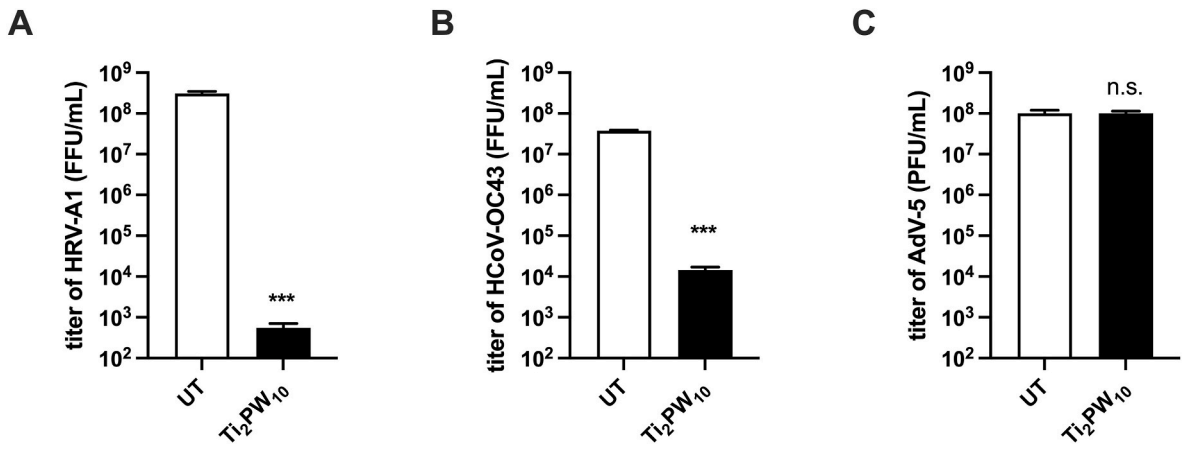

Fig. 1. Evaluation of the inhibition of the production of infectious viral progeny by Ti_2PW_{10}. Cells were infected with HRV-A1 **(A)**, HCoV-OC43 **(B)**, or AdV-5 **(C)** (MOI = 0.05) and treated with Ti_2PW_{10} at the respective EC_{99} dose. When CPE was evident in the untreated control wells, supernatants were collected and clarified virus was titrated accordingly. On the y-axis, viral titers are expressed as FFU/mL (HRV-A1, HCoV-OC43) or PFU/mL (AdV-5) and reported as mean ± SEM for three independent experiments. Treated and control samples were compared with the Student's t-test. n.s., not significant; *** = $p < 0.001$. UT, untreated.

Table 2
Antiviral activity of Ti_2PW_{10} on different cell lines and against different HRV and HCoV strains.

Virus	Compound	Type	Cell line	EC_{50} [a] (μM) (95% CI [b])	CC_{50} [c] (μM) (95% CI)	SI [d]
HRV	Ti_2PW_{10}	HRV-A1	HeLa	3.21 (2.71–3.81)	>2400	>747.7
			Huh7	3.01 (1.07–8.45)	>2400	>797.3
			A549	2.31 (1.56–3.42)	>2400	>1039
			Vero	10.4 (5.66–19.0)	>2400	>230.8
		HRV-B48	HeLa	73.7 (47.6–114.3)	>2400	>32.6
		HRV-A1 pleconaril-R	HeLa	2.38 (1.97–2.88)	>2400	>1008
		HRV-A1 rupintrivir-R	HeLa	2.33 (1.98–2.74)	>2400	>1030
	Pleconaril	HRV-A1	HeLa	0.44 (0.43–0.44)	698.4 (488.9–876.1)	1587
HCoV	Ti_2PW_{10}	HCoV-OC43	MRC-5	3.30 (3.12–3.50)	>2400	>727.3
			Huh7	35.4 (27.5–45.6)	>2400	>67.8
			A549	2.05 (1.79–2.36)	>2400	>1171
			Vero	8.52 (6.22–11.7)	>2400	>281.7
		HCoV-229E	MRC-5	0.92 (0.74–1.15)	>2400	>2609
		SARS-CoV-2 PsV	Huh7	4.05 (3.05–5.46)	>2400	>592.6
	Chloroquine	HCoV-OC43	MRC-5	0.19 (0.13–0.26)	169.3 (150.4–190.5)	891.1

n.a.: not assessable.
[a] EC_{50}: half maximal effective concentration.
[b] CI: 95% confidence interval.
[c] CC_{50}: half maximal cytotoxic concentration.
[d] SI: selectivity index.

pleconaril was tested against HRV-A1, while the known endocytosis inhibitor chloroquine was selected as reference compound to test against HCoV-OC43. As expected, HRV-A1 and HCoV-OC43 were inhibited by the respective antivirals, with EC_{50} values similar to those reported in literature (Hashem et al., 2020; Lacroix et al., 2014) (Table 2).

3.3. *Ti_2PW_{10} hampered virus entry into host cell*

Given the POM broad-spectrum antiviral activity, to explore its mechanism of action, we firstly investigated whether Ti_2PW_{10} exerted its activity directly on the viral particle or on the host cell. A virus inactivation assay showed that the POM did not exert intrinsic virucidal activity (Fig. S3), and pre-treatment assays demonstrated that Ti_2PW_{10} did not inhibit HRV-A1 or HCoV-OC43 infection, thus excluding a possible effect of the POM on the cell susceptibility to infection (Fig. 2A and C).

So, we focused on the possible inhibition of virus-host interactions or intracellular virus replicative steps. Through binding assays, we observed that the POM did not affect HCoV-OC43 binding to host cells, whereas it only slightly reduced HRV-A1 titer (Fig. 2B and D). Next, we investigated the virus entry and subsequent post-entry events. Fig. 2A and C shows that viral infectivity was inhibited in a dose-dependent manner when Ti_2PW_{10} was added during the virus entry, with EC_{50} values of 8.57 μM or 3.38 μM for HRV-A1 or HCoV-OC43, respectively. On the contrary, the POM was not active when added after viral entry, specifically after virus escape from late endosomes. The lack of activity of Ti_2PW_{10} in a post-entry experimental setting was determined by fixing and immunostaining cells using two different markers of viral replication, i.e., the dsRNA and the capsid protein VP2 (for HRV-A1) or nucleocapsid protein (for HCoV-OC43). Microscopical observation revealed the presence of both viral markers after post-entry antiviral treatment, indicating that the POM did not affect viral genome replication or the production of viral structural proteins (Fig. S4).

To determine whether the blockage of virus entry could take place outside the cell on the plasma membrane, covering common sites for virus binding and entry, we investigated the sub-cellular distribution of Ti_2PW_{10} using a rhodamine-labelled polyanion. The POM was able to penetrate intracellularly as soon as 5 min after treatment, distributing homogeneously in the cytoplasm at 1 h and 3 h post-treatment (Fig. 2E). Of note, the polyanion was not detected on the cytoplasmatic membrane.

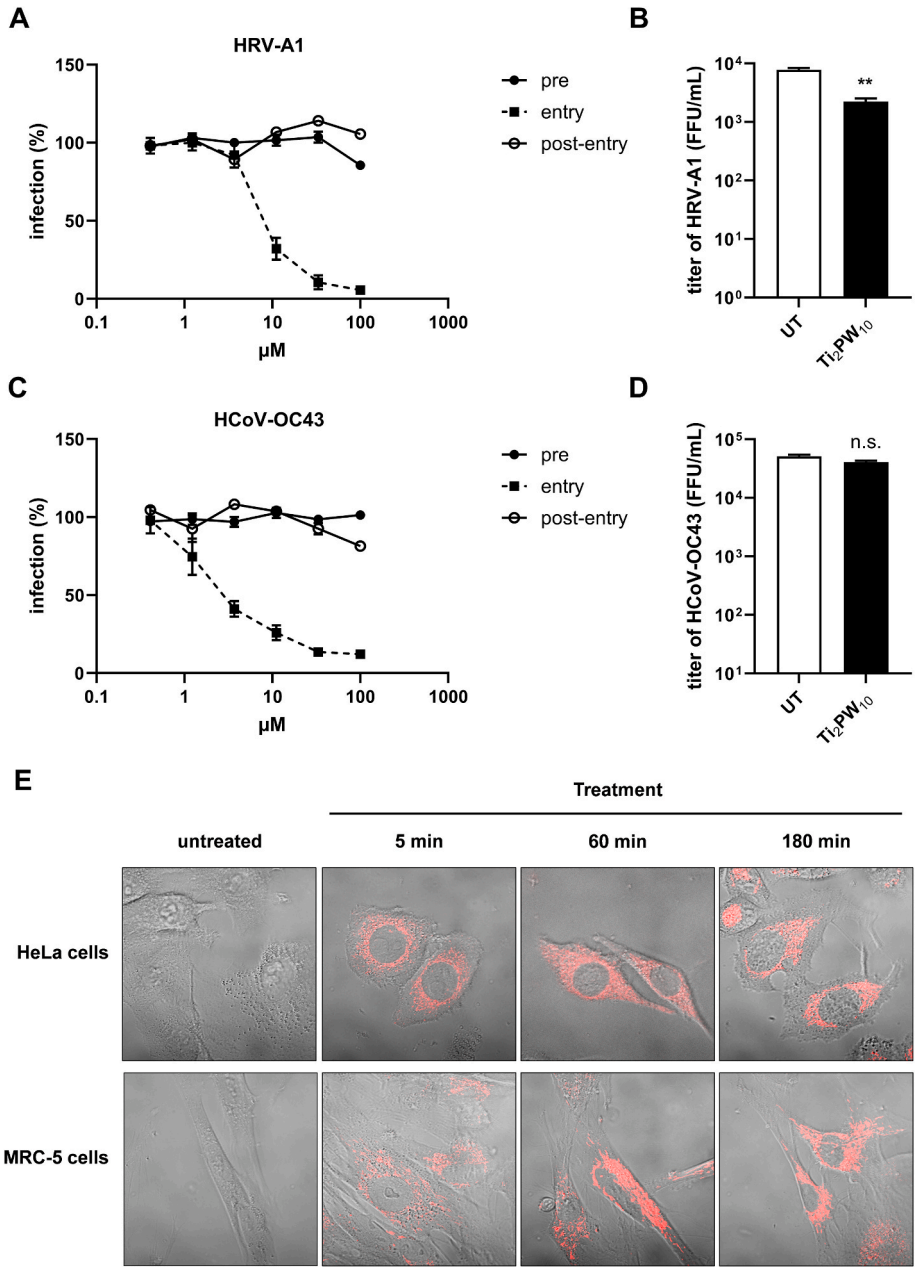

Fig. 2. Investigation of the antiviral mechanism of action of Ti_2PW_{10}. (A, C) Time-of-addition assays. Cells were treated with serial dilutions of Ti_2PW_{10} (100–0.4 μM) before infection (pre), during virus entry (entry) or after treatment with NH_4Cl (post-entry). Viral infectivity was assessed 24 h (HRV-A1) **(A)** or 16 h (HCoV-OC43) **(B)** after infection. The percent infection (%) was calculated by comparing treated and untreated wells. Error bars represent SEMs for three independent experiments. **(B, D)** Binding assays. The effect of Ti_2PW_{10} on the binding of HRV-A1 **(B)** or HCoV-OC43 **(D)** to host cells was assessed via binding assays. On y-axis, virus titers are expressed as focus forming units per mL (FFU/mL). Student's t-test was used to compare viral titers (n.s.: not significant; **: p-value <0.01). UT, untreated. **(E)** Ti_2PW_{10} cell uptake. Uninfected HeLa or MRC-5 cells were treated with fluorescent Ti_2PW_{10} for 5 min, 1 h, and 3 h. POM cell distribution in live cells was observed in red via confocal laser microscopy. Control sample (untreated) was incubated with culture medium alone. Magnification, 400 × .

3.4. Ti_2PW_{10} did not select resistant viral strains

As one of the main obstacles to antiviral therapy is the emergence of drug-resistant variants, we aimed to test the tendency of Ti_2PW_{10} to select resistant HRV-A1 or HCoV-OC43 in vitro via two different approaches.

Firstly, resistance development toward Ti_2PW_{10} was tested by serial passage approach, passaging HRV-A1 or HCoV-OC43 in the presence of increasing Ti_2PW_{10} concentrations (~EC_{50}) for 10 passages. As control, wildtype virus was passaged in parallel in absence of the compound. HRV-A1 and HCoV-OC43 remained highly sensitive to the polyanion up to the tenth passage of culture under selective pressure, as demonstrated by the absence of EC_{50} values shift between the resistant and wildtype strains (Fig. 3A–B, Tables S1 and S2).

Next, we investigated the development of resistance by an alternative method that allows to assess the frequency of resistant variants from the parental strain, i.e., clonal approach. The frequency of HRV-A1 resistant clones in Ti_2PW_{10}-treated samples was of 0.5% up to 7 d.p.i., indicating that it is highly unlikely to select resistance in the HRV quasispecies (Fig. 3C). Regarding HCoV-OC43, while no resistant clone was detected up to 3 d.p.i., starting from 4 d.p.i. we observed virus-induced CPE in a significant portion of Ti_2PW_{10}-treated samples (20.8% at 4 d.p.i., 61.5% at 7 d.p.i.) (Fig. 3D). Since treatment was performed only at day 0, this result could be ascribed to the possible

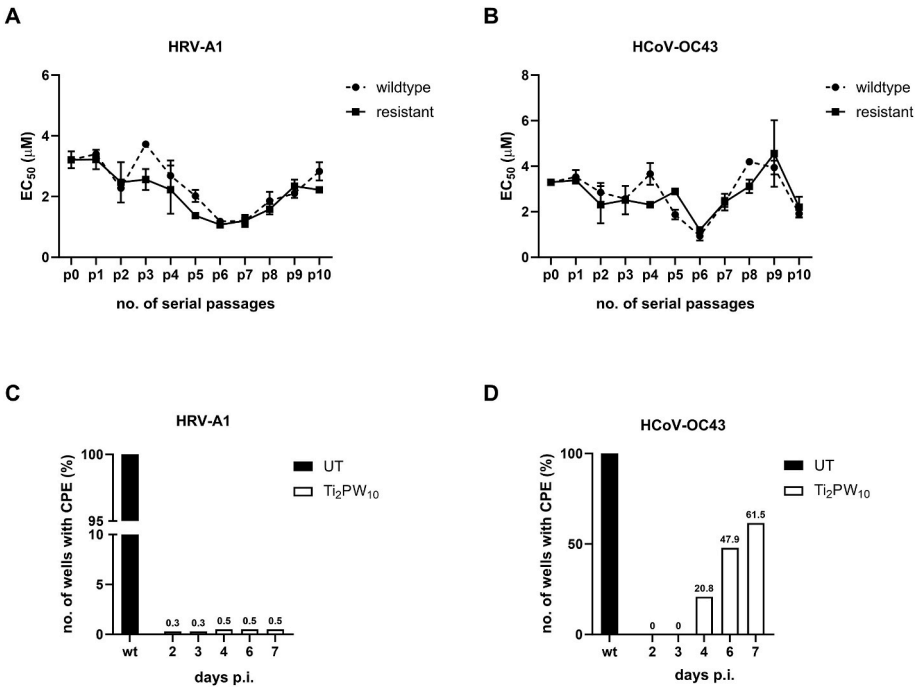

Fig. 3. Selection of resistant viral strains by Ti_2PW_{10}. (A, B) Serial passages approach. HRV-A1 **(A)** or HCoV-OC43 **(B)** was cultured for 10 passages on cell monolayers in the presence of sub-optimal concentrations of Ti_2PW_{10} (~EC_{50}). In parallel, wildtype virus was passaged without compound in the same experimental conditions. Virus sensitivity to Ti_2PW_{10} was tested at each passage for both wildtype and resistant virus by focus reduction assay, and expressed as EC_{50} on the y-axis. Error bars represent SDs of EC_{50}s for two replicates. **(C, D)** Clonal approach. A total of 384 wells (four 96-well plates) were seeded and 24 h later were infected with HRV-A1 **(C)** or HCoV-OC43 **(D)** in the presence of Ti_2PW_{10} at the respective EC_{99} dose. Each bar represents the percentage of wells that exhibited CPE compared to the total number of infected wells. One 96-well plate was infected and left untreated, as the control that exhibited CPE in 100% of wells (wt, wildtype). UT, untreated; days p.i.: days post-infection.

instability of Ti_2PW_{10} in the culture medium after prolonged incubation, coupled with differences in the replicative cycles of the two viruses. All selected variants in CPE-exhibiting wells, harvested and expanded under selective pressure, showed a <8-fold increase of EC_{50} values compared to the wildtype strain (Table S3).

3.5. *Ti_2PW_{10} inhibited viral replication in infected human nasal epithelia*

To validate the POM antiviral activity in a more challenging and predictive model, we carried out experiments on a 3D model of human nasal epithelium obtained from a pool of 14 healthy donors. HRV-A1 was selected as a model virus as we previously demonstrated its ability to replicate in nasal epithelia (Civra et al., 2022).

As outlined in Fig. 4A, the epithelia were infected with 50,000 FFU of HRV-A1 for 3h and treated with Ti_2PW_{10} every 24h, and newly produced virus was harvested daily and titrated. As shown in Fig. 4B, HRV yield naturally declined over time, in line with previous observations that showed the physiological clearance of HRV infection in highly differentiated human airway epithelial cells (Warner et al., 2019). Importantly, Ti_2PW_{10} inhibited HRV-A1 production at all time-points tested: at 24 h.p.i. viral titer was slightly reduced compared the untreated control (0.4-log reduction), increasing to 1.4-log reduction at 48 and 72 h.p.i., and reaching a 2.2-log reduction at 96 h.p.i. LDH assays on basal media collected daily from treated and untreated samples were performed to exclude toxicity of the POM on epithelia. Only a slight increase in cytotoxicity above the 5%-threshold was detected at 24 h.p.i., for all control and treated samples (Fig. 4C). This was likely ascribed to hypoxic stress caused by the overlay of media on the apical side of tissue inserts during the 3h-infection at day 0. Importantly, at later times, Ti_2PW_{10} treatment did not determine an increase in LDH release in treated samples, compared to untreated controls.

At 96 h.p.i., the tissues were fixed immediately after apical and basal harvests and subjected to H&E staining, to visualize any alteration in tissue morphology caused by antiviral treatment or infection (Fig. 4D). Consistently with recent studies and in line with results of LDH assays, HRV infection did not result in any overt sign of epithelial damage (Essaidi-Laziosi et al., 2018; Warner et al., 2019). More importantly, the treated sample showed a well-preserved morphology of the respiratory epithelium, with preservation of cilia, homogeneous pluri-stratification and no cyto-architectural alterations, similar to the untreated samples, indicating that the antiviral treatment was not cytotoxic.

3.6. *Mucoadhesive thermosensitive in situ gelling formulation of Ti_2PW_{10} was developed for nasal delivery*

Considering its potential use as antiviral drug for respiratory viral infections, a mucoadhesive thermosensitive *in situ* hydrogel formulation for the targeted nasal delivery of Ti_2PW_{10} was developed. The hydrogel demonstrated sol to gel transition at nasal cavity temperature (34 ± 1 °C). The addition of Ti_2PW_{10} did not modify the gelling properties of the formulation. Moreover, it behaved as a Newtonian fluid at 22 °C with constant viscosity values (114.84 ± 7.76 mPa s). Changes in the rheological properties of the samples were observed at 34 °C, with an increase of the viscosity that reached about 140000 mPa s at shear rate of 0.10 s^{-1}, confirming the formation of a hydrogel. The formulation showed a pH value of 6.30 ± 0.05, appropriate for nasal administration, and did not present hemolytic activity, confirming a good biocompatibility and tonicity values suitable for cell experiments.

The Ti_2PW_{10} formulation was assayed in vitro on cell cultures to test its antiviral activity. As shown in Fig. 5A, formulated Ti_2PW_{10} inhibited HRV-A1 and HCoV-OC43 infectivity in a dose-dependent manner, with EC_{50}s in the low micromolar range (1.20 μM and 0.76 μM, respectively) comparable to EC_{50} values obtained for Ti_2PW_{10} alone, while cell viability assays demonstrated that formulated Ti_2PW_{10} was not toxic to cells at antiviral effective doses (CC_{50}s > 600). Moreover, results from the virus yield reduction assays confirmed that formulated Ti_2PW_{10}

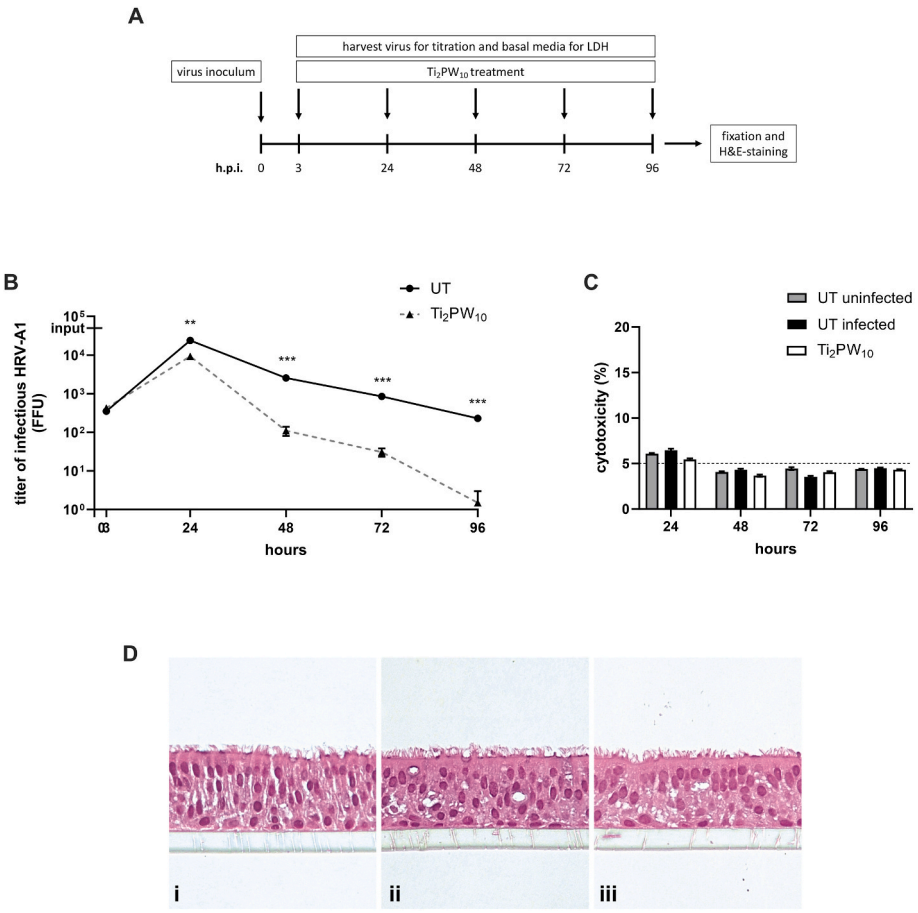

Fig. 4. Evaluation of the anti-HRV efficacy of Ti_2PW_{10} in a 3D reconstituted model of human nasal epithelium. (A) Schematic experimental protocol for the antiviral assays on human nasal epithelia. **(B)** Inhibitory activity of Ti_2PW_{10} against HRV-A1 on human nasal epithelia. Tissue inserts were infected with HRV-A1 (50,000 FFU, input) for 3 h, then treated with Ti_2PW_{10} after removal of inoculum and each 24 h after infection. Viral progeny was harvested every 24 h after infection and titrated (3, 24, 48, 72, 96 h); on y-axis, viral titers are expressed as FFU. Student's t-test was used to compare titers from untreated and treated wells at each time point. **(C)** Cytotoxic effect of Ti_2PW_{10} on human nasal epithelia. LDH assays were performed by sampling basal media every 24 h following HRV-A1 inoculation in presence or in absence of antiviral. Untreated uninfected tissue was used as control. Cytotoxicity is expressed on y-axis as percentage compared to a lysed control sample (100% cytotoxicity). 5% cytotoxicity threshold is set as the physiological cell turnover in 3D nasal epithelial cultures. **(D)** Representative images of human nasal epithelia. After 96 h, all samples were formalin-fixed and haematoxylin/eosin-stained. i) Untreated uninfected sample; ii) Untreated infected sample; iii) Ti_2PW_{10} treated sample.

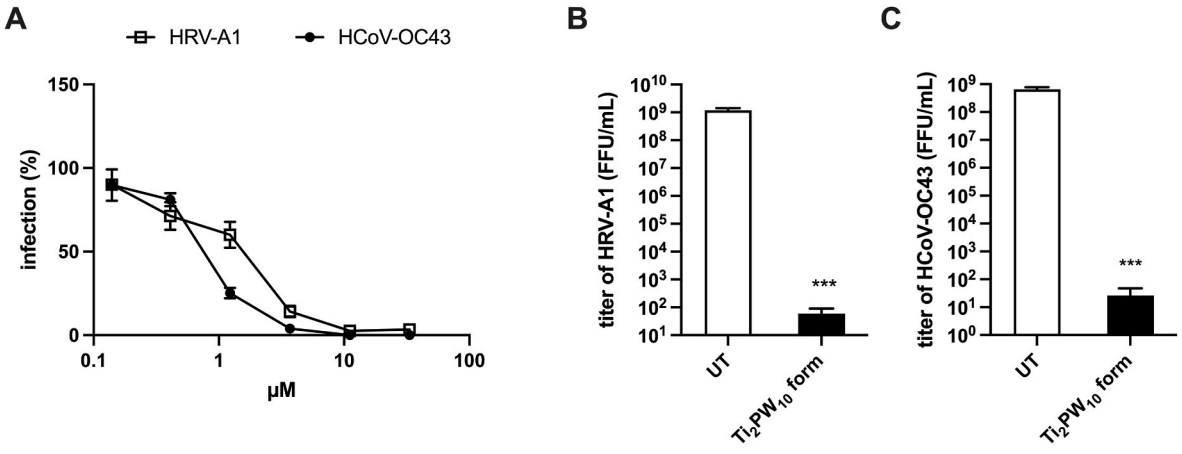

Fig. 5. Assessment of the antiviral activity of formulated Ti_2PW_{10} against HRV-A1 and HCoV-OC43. (A) Focus reduction assays. The antiviral activity of the POM formulation was evaluated treating cells with serial dilutions of Ti_2PW_{10} (100–0.4 μM) and assessing viral infectivity 24 h (HRV-A1) or 16 h (HCoV-OC43) after infection. Treated wells were compared to untreated controls to calculate the percent infection (%). Error bars represent SEMs for three replicates. **(B, C)** Virus yield reduction assays. Cells were infected with HRV-A1 **(B)** or HCoV-OC43 **(C)** (MOI = 0.05) and treated with Ti_2PW_{10} (EC_{99}). When full CPE developed in the untreated control wells, supernatants were collected, clarified and titrated. On the y-axis, viral titers are expressed as FFU/mL and reported as mean ± SEM for three independent experiments. Treated and control samples were compared with the Student's t-test. *** = $p < 0.001$. UT, untreated.

strongly inhibited the production of viral progeny, reducing the viral titer of 7.12 and 7.64 logs for HRV-A1 and HCoV-OC43 respectively, compared to untreated control (Fig. 5B–C).

4. Discussion

In this work, the Keggin-type POM Ti_2PW_{10} emerged as the most promising candidate from a mini-library of inorganic compounds, i.e., POMs, previously investigated for their various biological properties (Čolović et al., 2017, 2020; Ilyas et al., 2014; Iqbal et al., 2013). We found that Ti_2PW_{10} was able to inhibit the infectivity of various common human respiratory viruses, i.e., RSV-A2, HCoV-OC43, HRV-A1, and AdV-5, exhibiting good EC_{50}s (0.65–3.30 μM) and highly favorable CC_{50}s (>2400 μM). These data are consistent with previous works, demonstrating that the POM is effective against other viruses (namely zika virus, influenza virus and RSV) with comparable EC_{50} values in the same low micromolar range (Francese et al., 2019; Shigeta et al., 2006).

Further analyses focused only on Ti_2PW_{10}'s anti-coronaviral and anti-rhinoviral activity, as the POM was most active against these two viruses. We demonstrated that Ti_2PW_{10} exerted its antiviral activity independently of the cell type used and against different coronaviral and rhinoviral strains. Specifically, the polyanion was active against the wildtype human alpha-coronavirus HCoV-229E and a VSV-based pseudovirion of the beta-coronavirus SARS-CoV-2 (SARS-CoV-2-PsV). Since the not-replicating SARS-CoV-2-PsV surrogate model can only mimic early phases of the virus life cycle (i.e., attachment and entry), expressing on its surface SARS-CoV-2 Spike glycoprotein, we speculate that Ti_2PW_{10} acts by blocking the S protein-mediated attachment or entry of the pseudovirion into host cells. Indeed, a recent study identified Ti_2PW_{10} as a potential inhibitor of the interaction between the Spike glycoprotein of SARS-CoV-2 and the cell receptor ACE2 (Gil-Moles et al., 2021). Further experiments are required to confirm this activity, employing the wildtype SARS-CoV-2. Regarding anti-rhinoviral activity, POM inhibitory effect was also confirmed on HRV-A1 strains resistant to known anti-rhinoviral compound, i.e., protease 3C-targeting rupintrivir and capsid-binder pleconaril, suggesting a different target of Ti_2PW_{10}'s antiviral action. Interestingly, Ti_2PW_{10} inhibited less effectively the related HRV-B48, with an EC_{50} of 39.5 μM. This result might be ascribed to the different host cell receptors that HRV-A1 and HRV-B48 use for the entry, respectively the low-density lipoprotein receptor (LDLR) or the intracellular adhesion molecule 1 (ICAM-1) (Vlasak et al., 2005).

Although further studies are needed to identify the target/s of POM antiviral activity, preliminary experiments confirmed the above-hypothesized blockage of early stages of viral life cycle by Ti_2PW_{10}. We demonstrated that the main target of POM antiviral activity is the HCoV-OC43 and HRV-A1 entry into host cells, specifically after virus binding to host cell receptor and before virus release from late endosomes. This activity is in accordance with recent literature, that identified Ti_2PW_{10} as an entry inhibitor of several other human viruses, including ZIKV, HIV, and HSV-2 (Dan and Yamase, 2006; Francese et al., 2019; Take et al., 1991). Moreover, Shigeta et al. showed that Ti_2PW_{10} inhibited FluV-A infection by hampering the fusion between viral envelope and host cell membrane, not affecting the binding of FluV-A to cellular receptors (Shigeta et al., 2006).

A major obstacle in antiviral research is the emergence of drug-resistant variants, particularly for RNA viruses due to their high mutation rate determined by the lack of proof-reading activity of the viral RNA-dependent RNA polymerase (10^{-6}-10^{-4} nucleotide substitutions per cell infection) (Bordería et al., 2016; Coultas et al., 2021; Sanjuán and Domingo-Calap, 2016). Here, we demonstrated via a serial passage approach that Ti_2PW_{10} does not exert selective pressure on HCoV-OC43 and HRV-A1, as the emergence of resistant variants was not documented up to the tenth passage. Concurrently, the clonal approach indicated that the virus quasispecies contained only few variants with some natural level of resistance, albeit not clinically relevant (Dycke et al., 2021; Lacroix et al., 2015).

To determine the therapeutic potential of a candidate antiviral, we tested the compound's antiviral efficacy in a predictive in vitro model, that is, a 3D human nasal epithelial tissue cultured at the air-liquid interface, exhibiting mucociliary clearance and secretion of defensive molecules, susceptible to infection of various human respiratory viruses (Boda et al., 2018; Civra et al., 2022). Treatment with Ti_2PW_{10} was able to accelerate the clearance of HRV-A1 in infected epithelia, reaching a titer reduction of 2.2-log compared to control at 96 h.p.i. Importantly, cytotoxicity assays and H&E staining of epithelia revealed that antiviral treatment did not cause tissue distress or damage.

Despite POMs wide spectrum of biological activities, the possibility of acute or long-term toxic effects has so far been the reason behind for the lack of interest in the further development of these candidate drugs. Concerning Ti_2PW_{10}, Čolović et al. showed that the polyanion cannot be considered highly toxic following a toxicity evaluation of orally-administered *Wistar albino* rats (Čolović et al., 2017). A more complex toxicological study involving the assessment of long-term side effects, and exploring different routes of administration and drug delivery strategies, will be necessary for its further selection as potential candidate in antiviral therapy. In this context, a mucoadhesive thermosensitive *in situ* hydrogel formulation for the nasal delivery of Ti_2PW_{10} was herein synthesized and characterized, with the aim of increasing the concentration of the drug at the site of infection, while limiting systemic drug exposure. Indeed, previous studies reported POMs' organic functionalization (Flütsch et al., 2011) and their incorporation in nanocarriers, such as silica nanospheres (Cao et al., 2017), polymeric nanoparticles (Croce et al., 2019) and in hydrogel matrices (Pandya et al., 2024) as strategies to improve the POM biocompatibility, physiological stability and activity. In particular, thermosensitive hydrogel formulations represent a promising approach for POM nasal administration. The increase of viscosity after gelation can prevent the rapid drainage from nasal cavity experienced by liquid formulations, limiting the rapid mucociliary clearance (Vigani et al., 2020; Wang et al., 2019). In addition, mucoadhesive properties can be exploited to prolong the residence time at the nasal site and favor POM antiviral activity.

4.1. Conclusions

Here, we demonstrated that the Keggin-type polyanion Ti_2PW_{10} is endowed with broad-spectrum activity against various of human respiratory viruses acting as entry inhibitor, alongside with absence of development of antiviral resistance, high cytocompatibility and antiviral activity on ciliated human nasal epithelia. Altogether, these several competitive advantages make Ti_2PW_{10} a promising starting point for a drug candidate against respiratory viral infections.

Funding

This work was supported by EU funding within the MUR PNRR Extended Partnership Initiative on Emerging Infectious Diseases (Project no. PE00000007, INF-ACT). The funders had no role in the study design, the data collection and interpretation, or the decision to submit the work for publication.

CRediT authorship contribution statement

Irene Arduino: Writing – original draft, Investigation, Formal analysis. **Rachele Francese:** Resources, Investigation. **Andrea Civra:** Methodology. **Elisa Feyles:** Investigation. **Monica Argenziano:** Resources, Investigation. **Marco Volante:** Investigation. **Roberta Cavalli:** Supervision, Conceptualization. **Ali M. Mougharbel:** Investigation. **Ulrich Kortz:** Writing – review & editing, Conceptualization. **Manuela Donalisio:** Writing – review & editing, Supervision, Conceptualization. **David Lembo:** Writing – review & editing, Supervision, Funding acquisition, Conceptualization.

Declaration of competing interest

The authors declare that they have no known competing financial interests or personal relationships that could have appeared to influence the work reported in this paper.

Data availability

Data will be made available on request.

Acknowledgements

None.

Glossary

Polyoxometalate Discrete, anionic metal-oxo complexes of early d-block metal ions in high oxidation states, such as W^{VI}, Mo^{VI}, and V^{V}

Appendix A. Supplementary data

Supplementary data to this article can be found online at https://doi.org/10.1016/j.antiviral.2024.105897.

References

Boda, B., Benaoudia, S., Huang, S., Bonfante, R., Wiszniewski, L., Tseligka, E.D., Tapparel, C., Constant, S., 2018. Antiviral drug screening by assessing epithelial functions and innate immune responses in human 3D airway epithelium model. Antivir. Res. 156, 72–79. https://doi.org/10.1016/J.ANTIVIRAL.2018.06.007.

Bordería, A.V., Rozen-Gagnon, K., Vignuzzi, M., 2016. Fidelity variants and RNA quasispecies. Curr. Top. Microbiol. Immunol. 392, 303–322. https://doi.org/10.1007/82_2015_483.

Cagno, V., Donalisio, M., Civra, A., Cagliero, C., Rubiolo, P., Lembo, D., 2015. In vitro evaluation of the antiviral properties of Shilajit and investigation of its mechanisms of action. J. Ethnopharmacol. 166, 129–134. https://doi.org/10.1016/J.JEP.2015.03.019.

Cagno, V., Sgorbini, B., Sanna, C., Cagliero, C., Ballero, M., Civra, A., Donalisio, M., Bicchi, C., Lembo, D., Rubiolo, P., 2017. In vitro anti-herpes simplex virus-2 activity of Salvia desoleana Atzei & V. Picci essential oil. PLoS One 12, 1–12. https://doi.org/10.1371/journal.pone.0172322.

Cao, H., Li, C., Qi, W., Meng, X., Tian, R., Qi, Y., Yang, W., Li, J., 2017. Synthesis, cytotoxicity and antitumour mechanism investigations of polyoxometalate doped silica nanospheres on breast cancer MCF-7 cells. PLoS One 12 (7), e0181018. https://doi.org/10.1371/journal.pone.0181018.

Chen, Y.Q., 1997. On the Existence of Abelian hadamard difference sets and a new family of difference sets. Finite Fields Their Appl. 3, 234–256. https://doi.org/10.1006/FFTA.1997.0184.

Civra, A., Costantino, M., Cavalli, R., Adami, M., Volante, M., Poli, G., Lembo, D., 2022. 27-Hydroxycholesterol inhibits rhinovirus replication in vitro and on human nasal and bronchial histocultures without selecting viral resistant variants. Antivir. Res. 204, 105368 https://doi.org/10.1016/j.antiviral.2022.105368.

Civra, A., Francese, R., Gamba, P., Testa, G., Cagno, V., Poli, G., Lembo, D., 2018. 25-Hydroxycholesterol and 27-hydroxycholesterol inhibit human rotavirus infection by sequestering viral particles into late endosomes. Redox Biol. 19, 318–330. https://doi.org/10.1016/J.REDOX.2018.09.003.

Čolović, M.B., Lacković, M., Lalatović, J., Mougharbel, A.S., Kortz, U., Krstić, D.Z., 2020. Polyoxometalates in biomedicine: update and overview. Curr. Med. Chem. 27, 362–379. https://doi.org/10.2174/0929867326666190827153532.

Čolović, M.B., Medić, B., Ćetković, M., Kravić Stevović, T., Stojanović, M., Ayass, W.W., Mougharbel, A.S., Radenković, M., Prostran, M., Kortz, U., Krstić, D.Z., 2017. Toxicity evaluation of two polyoxotungstates with anti-acetylcholinesterase activity. Toxicol. Appl. Pharmacol. 333, 68–75. https://doi.org/10.1016/J.TAAP.2017.08.010.

Coultas, J.A., Cafferkey, J., Mallia, P., Johnston, S.L., 2021. Experimental antiviral therapeutic studies for human rhinovirus infections. J. Exp. Pharmacol. 13, 645–659. https://doi.org/10.2147/JEP.S255211.

Croce, M., Conti, S., Maake, C., Patzke, G.R., 2019. Nanocomposites of polyoxometalates and chitosan-based polymers as tuneable anticancer agents. Eur. J. Inorg. Chem. (3–4), 348–356. https://doi.org/10.1002/ejic.201800268.

Dan, K., Yamase, T., 2006. Prevention of the interaction between HVEM, herpes virus entry mediator, and gD, HSV envelope protein, by a Keggin polyoxotungstate, PM-19. Biomed. Pharmacother. 60, 169–173. https://doi.org/10.1016/J.BIOPHA.2006.02.005.

Domaille, P.J., Knoth, W.H., 1983. Ti2W10PO40 and [CpFe(CO)2Sn]2W10PO5-38. Preparation, properties, and structure determination by tungsten-183 NMR. Inorg. Chem. 22, 818–822. https://doi.org/10.1021/IC00147A023.

Dycke, J. Van, Rymenants, J., Neyts, J., Rocha-Pereira, J., 2021. Assessment of the anti-norovirus activity in cell culture using the mouse norovirus: early mechanistic studies. Antivir. Chem. Chemother. 29 https://doi.org/10.1177/20402066211025175.

Enderle, A.G., Bosso, M., Groß, R., Heiland, M., Bollini, M., Culzoni, M.J., Kirchhoff, F., Münch, J., Streb, C., 2021. Increased in vitro anti-HIV activity of caffeinium-functionalized polyoxometalates. ChemMedChem 16, 2727–2730. https://doi.org/10.1002/CMDC.202100281.

Esneau, C., Duff, A.C., Bartlett, N.W., 2022. Understanding rhinovirus circulation and impact on illness, 2022 Viruses 14. https://doi.org/10.3390/V14010141. Page 141 14, 141.

Essaidi-Laziosi, M., Brito, F., Benaoudia, S., Royston, L., Cagno, V., Fernandes-Rocha, M., Piuz, I., Zdobnov, E., Huang, S., Constant, S., Boldi, M.O., Kaiser, L., Tapparel, C., 2018. Propagation of respiratory viruses in human airway epithelia reveals persistent virus-specific signatures. J. Allergy Clin. Immunol. 141, 2074–2084. https://doi.org/10.1016/J.JACI.2017.07.018.

Fausto, A., Otter, C.J., Bracci, N., Weiss, S.R., 2023. Improved culture methods for human coronaviruses HCoV-OC43, HCoV-229E, and HCoV-NL63. Curr. Protoc. 3, e914. https://doi.org/10.1002/CPZ1.914.

Feder, A.F., Harper, K.N., Brumme, C.J., Pennings, P.S., 2021. Understanding patterns of HIV multi-drug resistance through models of temporal and spatial drug heterogeneity. Elife 10. https://doi.org/10.7554/ELIFE.69032.

Flütsch, A., Schroeder, T., Grütter, M.G., Patzke, G.R., 2011. HIV-1 protease inhibition potential of functionalized polyoxometalates. Bioorg. Med. Chem. Lett 21 (4), 1162–1166. https://doi.org/10.1016/j.bmcl.2010.12.103.

Francese, R., Civra, A., Rittà, M., Donalisio, M., Argenziano, M., Cavalli, R., Mougharbel, A.S., Kortz, U., Lembo, D., 2019. Anti-zika virus activity of polyoxometalates. Antivir. Res. 163, 29–33. https://doi.org/10.1016/j.antiviral.2019.01.005.

Freymuth, F., Vabret, A., Rozenberg, F., Dina, J., Petitjean, J., Gouarin, S., Legrand, L., Corbet, S., Brouard, J., Lebon, P., 2005. Replication of respiratory viruses, particularly influenza virus, rhinovirus, and coronavirus in HuH7 hepatocarcinoma cell line. J. Med. Virol. 77, 295–301. https://doi.org/10.1002/JMV.20449.

Gil-Moles, M., Türck, S., Basu, U., Pettenuzzo, A., Bhattacharya, S., Rajan, A., Ma, X., Büssing, R., Wölker, J., Burmeister, H., Hoffmeister, H., Schneeberg, P., Prause, A., Lippmann, P., Kusi-Nimarko, J., Hassell-Hart, S., McGown, A., Guest, D., Lin, Y., Notaro, A., Vinck, R., Karges, J., Cariou, K., Peng, K., Qin, X., Wang, X., Skiba, J., Szczupak, Ł., Kowalski, K., Schatzschneider, U., Hemmert, C., Gornitzka, H., Milaeva, E.R., Nazarov, A.A., Gasser, G., Spencer, J., Ronconi, L., Kortz, U., Cinatl, J., Bojkova, D., Ott, I., 2021. Metallodrug profiling against SARS-CoV-2 target proteins identifies highly potent inhibitors of the S/ACE2 interaction and the papain-like protease PLpro. Chem. Eur J. 27, 17928–17940. https://doi.org/10.1002/CHEM.202103258.

Grace, M., Colosia, A., Wolowacz, S., Panozzo, C., Ghaswalla, P., 2023. Economic burden of respiratory syncytial virus infection in adults: a systematic literature review. J. Med. Econ. 26, 742–759. https://doi.org/10.1080/13696998.2023.2213125.

Hadian, S.A., Rezayatmand, R., 2022. Economic impact of acute respiratory disease pandemics: a scoping review. J. Res. Med. Sci. 27 https://doi.org/10.4103/JRMS.JRMS_870_21.

Harrington, W.N., Kackos, C.M., Webby, R.J., 2021. The evolution and future of influenza pandemic preparedness. Exp. Mol. Med. 535 (53), 737–749. https://doi.org/10.1038/s12276-021-00603-0, 2021.

Hashem, A.M., Alghamdi, B.S., Algaissi, A.A., Alshehri, F.S., Bukhari, A., Alfaleh, M.A., Memish, Z.A., 2020. Therapeutic use of chloroquine and hydroxychloroquine in COVID-19 and other viral infections: a narrative review. Trav. Med. Infect. Dis. 35, 101735 https://doi.org/10.1016/J.TMAID.2020.101735.

Ilyas, Z., Shah, H.S., Al-Oweini, R., Kortz, U., Iqbal, J., 2014. Antidiabetic potential of polyoxotungstates: in vitro and in vivo studies. Metallomics 6, 1521–1526. https://doi.org/10.1039/c4mt00106k.

Iqbal, J., Barsukova-Stuckart, M., Ibrahim, M., Ali, S.U., Khan, A.A., Kortz, U., 2013. Polyoxometalates as potent inhibitors for acetyl and butyrylcholinesterases and as potential drugs for the treatment of Alzheimer's disease. Med. Chem. Res. 22, 1224–1228. https://doi.org/10.1007/s00044-012-0125-8.

Jin, Y.H., Min, J.S., Kwon, S., 2023. Cardamonin as a p38 MAPK signaling pathway activator inhibits human coronavirus OC43 infection in human lung cells, 2023 Nutrition 15. https://doi.org/10.3390/NU15061335, 1335 15, 1335.

Jurgeit, A., McDowell, R., Moese, S., Meldrum, E., Schwendener, R., Greber, U.F., 2012. Niclosamide is a proton carrier and targets acidic endosomes with broad antiviral effects. PLoS Pathog. 8, e1002976 https://doi.org/10.1371/JOURNAL.PPAT.1002976.

Kaptein, S.J.F., Goethals, O., Kiemel, D., Marchand, A., Kesteleyn, B., Bonfanti, J.F., Bardiot, D., Stoops, B., Jonckers, T.H.M., Dallmeier, K., Geluykens, P., Thys, K., Crabbe, M., Chatel-Chaix, L., Münster, M., Querat, G., Touret, F., de Lamballerie, X., Raboisson, P., Simmen, K., Chaltin, P., Bartenschlager, R., Van Loock, M., Neyts, J., 2021. A pan-serotype dengue virus inhibitor targeting the NS3-NS4B interaction. Nature 598, 504–509. https://doi.org/10.1038/S41586-021-03990-6.

Lacroix, C., George, S., Leyssen, P., Hilgenfeld, R., Neyts, J., 2015. The enterovirus 3C protease inhibitor SG85 efficiently blocks rhinovirus replication and is not cross-resistant with rupintrivir. Antimicrob. Agents Chemother. 59, 5814–5818. https://doi.org/10.1128/AAC.00534-15.

Lacroix, C., Querol-Audí, J., Roche, M., Franco, D., Froeyen, M., Guerra, P., Terme, T., Vanelle, P., Verdaguer, N., Neyts, J., Leyssen, P., 2014. A novel benzonitrile analogue inhibits rhinovirus replication. J. Antimicrob. Chemother. 69, 2723–2732. https://doi.org/10.1093/JAC/DKU200.

Lee, N., Hurt, A.C., 2018. Neuraminidase inhibitor resistance in influenza: a clinical perspective. Curr. Opin. Infect. Dis. 31, 520–526. https://doi.org/10.1097/QCO.0000000000000498.

Li, Q., Zhang, H., Qi, Y., Wang, J., Li, J., Niu, J., 2019. Antiviral effects of a niobium-substituted heteropolytungstate on hepatitis B virus-transgenic mice. Drug Dev. Res. 80, 1062–1070. https://doi.org/10.1002/DDR.21586.

Ljubin-Sternak, S., Meštrović, T., 2023. Rhinovirus—a true respiratory threat or a common inconvenience of childhood?, 2023 Viruses 15. https://doi.org/10.3390/V15040825, 825 15, 825.

Ljubin-Sternak, S., Meštrović, T., Lukšić, I., Mijač, M., Vraneš, J., 2021. Seasonal coronaviruses and other neglected respiratory viruses: a global perspective and a local snapshot. Front. Public Health 9, 691163. https://doi.org/10.3389/FPUBH.2021.691163.

Ma, Y., Frutos-Beltrán, E., Kang, D., Pannecouque, C., De Clercq, E., Menéndez-Arias, L., Liu, X., Zhan, P., 2021. Medicinal chemistry strategies for discovering antivirals effective against drug-resistant viruses. Chem. Soc. Rev. 50, 4514–4540. https://doi.org/10.1039/D0CS01084G.

Maglione, A., Francese, R., Arduino, I., Rosso, R., Matta, M., Rolla, S., Lembo, D., Clerico, M., 2023. Long-lasting neutralizing antibodies and T cell response after the third dose of mRNA anti-SARS-CoV-2 vaccine in multiple sclerosis. Front. Immunol. 14, 1–12. https://doi.org/10.3389/fimmu.2023.1205879.

Milani, M., Donalisio, M., Bonotto, R.M., Schneider, E., Arduino, I., Boni, F., Lembo, D., Marcello, A., Mastrangelo, E., 2021. Combined in silico and in vitro approaches identified the antipsychotic drug lurasidone and the antiviral drug elbasvir as SARS-CoV2 and HCoV-OC43 inhibitors. Antivir. Res. 189, 105055 https://doi.org/10.1016/j.antiviral.2021.105055.

Pandya, V.M., Goswami, D., Joshi, S.A., 2024. Biopolymer hydrogel matrices for the stabilization and in-vitro delivery of anti-cancer polyoxometalate [CoW11O39 (CpTi)] 7. J. Macromol. Sci. Part A 61 (2), 131–142. https://doi.org/10.1080/10601325.2024.2308547.

Qi, Yue, Han, L., Qi, Yanfei, Jin, X., Zhang, B., Niu, J., Zhong, J., Xu, Y., 2020. Anti-flavivirus activity of polyoxometalate. Antivir. Res. 179 https://doi.org/10.1016/J.ANTIVIRAL.2020.104813.

Qi, Yue, Xiang, Y., Wang, J., Qi, Yanfei, Li, J., Niu, J., Zhong, J., 2013. Inhibition of hepatitis C virus infection by polyoxometalates. Antivir. Res. 100, 392–398. https://doi.org/10.1016/J.ANTIVIRAL.2013.08.025.

Richman, D.D., 2006. Antiviral drug resistance. Antivir. Res. 71, 117–121. https://doi.org/10.1016/J.ANTIVIRAL.2006.03.004.

Romero-Tapia, S. de J., Guzmán Priego, C.G., Del-Río-Navarro, B.E., Sánchez-Solis, M., 2023. Advances in the relationship between respiratory viruses and asthma. J. Clin. Med. 12 https://doi.org/10.3390/jcm12175501.

Sanjuán, R., Domingo-Calap, P., 2016. Mechanisms of viral mutation. Cell. Mol. Life Sci. 73, 4433–4448. https://doi.org/10.1007/S00018-016-2299-6, 2016 7323.

Schmidt, K.J., Schrobilgen, G.J., Sawyer, J.F., Iucr, 1986. Hexasodium hexatungstotellurate(VI) 22-hydrate. Acta Crystallogr. 42, 1115–1118. https://doi.org/10.1107/S0108270186093204.

Shigeta, S., Mori, S., Yamase, T., Yamamoto, Norio, Yamamoto, Naoki, 2006. Anti-RNA virus activity of polyoxometalates. Biomed. Pharmacother. 60, 211–219. https://doi.org/10.1016/j.biopha.2006.03.009.

Take, Y., Tokutake, Y., Inouye, Y., Yoshida, T., Yamamoto, A., Yamase, T., Nakamura, S., 1991. Inhibition of proliferation of human immunodeficiency virus type 1 by novel heteropolyoxotungstates in vitro. Antivir. Res. 15, 113–124. https://doi.org/10.1016/0166-3542(91)90029-Q.

Thibaut, H.J., De Palma, A.M., Neyts, J., 2012. Combating enterovirus replication: state-of-the-art on antiviral research. Biochem. Pharmacol. 83, 185–192. https://doi.org/10.1016/J.BCP.2011.08.016.

Vigani, B., Rossi, S., Sandri, G., Bonferoni, M.C., Caramella, C.M., Ferrari, F., 2020. Recent advances in the development of in situ gelling drug delivery systems for non-parenteral administration routes. Pharmaceutics 12 (9), 859. https://doi.org/10.3390/pharmaceutics12090859.

Vlasak, M., Roivainen, M., Reithmayer, M., Goesler, I., Laine, P., Snyers, L., Hovi, T., Blaas, D., 2005. The minor receptor group of human rhinovirus (HRV) includes HRV23 and HRV25, but the presence of a lysine in the VP1 HI loop is not sufficient for receptor binding. J. Virol. 79, 7389–7395. https://doi.org/10.1128/JVI.79.12.7389-7395.2005.

Wang, J., Liu, Y., Xu, K., Qi, Y., Zhong, J., Zhang, K., Li, J., Wang, E., Wu, Z., Kang, Z., 2014. Broad-spectrum antiviral property of polyoxometalate localized on a cell surface. ACS Appl. Mater. Interfaces 6, 9785–9789. https://doi.org/10.1021/AM502193F.

Wang, Q., Zuo, Z., Cheung, C.K.C., Leung, S.S.Y., 2019. Updates on thermosensitive hydrogel for nasal, ocular and cutaneous delivery. Int. J. Pharm. 559, 86–101. https://doi.org/10.1016/j.ijpharm.2019.01.030.

Warner, S.M., Wiehler, S., Michi, A.N., Proud, D., 2019. Rhinovirus replication and innate immunity in highly differentiated human airway epithelial cells. Respir. Res. 20, 1–13. https://doi.org/10.1186/S12931-019-1120-0.